J Mater Sci: Mater Electron (2017) 28:9566–9574
DOI 10.1007/s10854-017-6704-1

Characterization of sodium lead silicate glasses containing low and high levels of Fe_2O_3 and effect of its replacement for Na_2O

Reham M. M. Morsi[1] · Safeya Ibrahim[2] · Morsi M. Morsi[2]

Received: 11 January 2017 / Accepted: 3 March 2017 / Published online: 29 March 2017

Abstract Glass of the composition (mol%) (25-x) Na_2O–xFe_2O_3–25PbO–50SiO_2, $x=0$, 0.25, 0.5, 1, 3, 5, 7, 10, 15, 16 and 20 (mol%) were prepared by the melt quenching method. The effect of replacing Fe_2O_3 for Na_2O on the optical, structural, electrical and dielectric properties was studied. Experimental and theoretical density and XRD of the samples were also reported. Pb^{2+}, Fe^{2+} and Fe^{3+} ions contributed to the UV-cut off and the developed bands in the visible and near IR regions. FTIR revealed the decrease of the SiO_4 and increase of FeO_4 units. XRD indicated change in the glass structure above 15 mol% Fe_2O_3. The electrical conduction seems to occur by ionic and electronic controlled electron hopping between Fe^{2+} and Fe^{3+} sites. The activation energy of ionic conduction decreased from 1.74 eV for un-replaced Na_2O sample to 0.16 eV for sample with 16 mol% Fe_2O_3 at 1 MHz. Samples with 16 and 20 (mol% Fe_2O_3) showed ε' values in the range from 115 to 186 and from 34 to 66, respectively. These results present promising candidates for the studied glasses to be used as energy storage materials in electronic devices.

1 Introduction

Lead silicate glasses are applied in many different areas such as video-screen manufacturing, electrode glass production, ophthalmic, biotechnology and radiation protection [1]. Glasses containing Fe_2O_3 are also used in electrochemical, electronic and electro-optic devices [2]. These glasses have very interesting structure and offer properties such as high value of the refractive index, low absorption in the visible region of the spectrum, an improved chemical stability and brightness [3, 4].

Lead oxide (PbO) is unique in its influence on the structure of glasses. Such interesting properties of these glasses are mainly due to the high polarizability and the relatively low field strengths of Pb cations as compared to other conventional glass formers such as SiO_2 and GeO_2 [5]. In lead silicate glasses, Pb^{2+} ions act as glass formers when PbO is present in high quantities and as network modifiers when lead oxide is present in lower concentrations [6]. When the structural role of Pb^{2+} is changed a considerable modification in the local environment of the silicate network occurs. It was suggested [7] that SiO_2 is the main glass former in the lead silicate glasses when PbO is present up to 40% where PbO is mainly present as glass modifier. When PbO is present over and above this concentration the polymeric chains of PbO_4 pyramids were found to be connected through silicate tetrahedra in the glass. However, it is reported [8] that, the PbO_4 groups are dominating for any concentration of PbO and at low concentrations the co-existence of the PbO_4 groups and PbO_3 pyramids is possible.

Recent works have shown that principal features for Fe-containing glasses are dependent on the valence states of iron ions and their coordination in the glass network [9, 10]. When iron oxides are introduced into glasses, iron ions exist as equilibrium between the yellow ferric ion, Fe^{3+}, and the blue ferrous ion, Fe^{2+} [11]. Most of ferrous iron is believed to exist in octahedral coordination as a network modifier [12]. On the other hand, ferric iron may exist in

✉ Reham M. M. Morsi
morsi_reham@yahoo.com

[1] Physical Chemistry Department, National Research Centre, 33 E l Bohoth St. (former El Tahrir St.), Dokki, Giza 12622, Egypt

[2] Glass Research Department, National Research Centre, 33 E l Bohoth St. (former El Tahrir St.), Dokki, Giza 12622, Egypt

four fold tetrahedral, and/or six fold octahedral coordination [13–16]. The oxidation states of iron were extensively studied in silicate glasses and melts [17–19].

Limited ternary systems of silicate glasses containing Fe_2O_3 are investigated. Iron doped sodium lead borate glasses were studied by electrical measurements and Mössbauer spectroscopy [20]. Cerium lead borate glasses doped with iron oxide [21] and lithium lead borate glasses doped with silver oxide [22] were investigated. Electron paramagnetic resonance and optical study was performed for alkali lead tetra borate glasses doped with iron oxide [23]. The transport properties of Fe_2O_3–PbO–B_2O_3 glasses were studied by Sanjay et al. [5]. The optical absorption properties of lead silicate glasses containing high concentrations of iron oxide were studied by Ookawa et al. [24]. The electronic conductivity, XRD and atomic force microscopy and magnetic force microscopy in the SiO_2–PbO–Fe_2O_3 glass were investigated [25]. Lead oxyfluoro silicate glasses containing iron ions were subjected to optical absorption, ESR, FTIR spectral investigations [6]. The role of Fe in a series of Fe_2O_3–PbO–SiO_2–Na_2O glasses in occupying octahedral or tetrahedral sites is investigated [26]. The dielectric constant of the system $xFe_2O_3 \cdot (1-x)PbO \cdot SiO_2$ in addition to IR and Raman spectra have been reported [27].

In previous studies on **e**ffect of replacing Fe_2O_3 for Na_2O on the chemical durability and glass structure of glass of composition $(25-x)\ Na_2O-x-Fe_2O_3-25PbO-50SiO_2$ has been investigated [28]. The aim of the present work is to extend such investigation to investigate the electrical and dielectric properties which have been noticed to receive less attention. The optical and physical properties will also be correlated with the glass structures of glasses.

2 Materials and methods

Glass samples of the composition (mol %) $(25-x)\ Na_2O-xFe_2O_3-25PbO-50SiO_2$ were prepared by the melt quenching method. Samples with x = 0, 0.25, 0.5, 1, 3, 5, 7, 10, 15, 16, and 20, were denoted as F0, F0.25, F0.5, F1, F3, F5, F7, F10, F15, F16, and F20, respectively. Table 1 lists the nominal composition of the studied glass samples. Chemically pure Na_2CO_3, Fe_2O_3 and Pb_3O_4 and washed silica sand were used as materials for glass batch preparation. The batch materials in the appropriate amounts were thoroughly mixed and melted in porcelain crucibles at a temperature of 1200 °C, using electrically heated furnace. Melting was continued under normal atmospheric conditions for 2 h after the last addition of the batch constituents. The melts were swirled about for every 30 min to ensure homogeneity and the melts were cast in rectangular forms, and samples were immediately transferred to electrically heated furnace at 450 °C. The furnace was switched off and left to cool to room temperature. Some of the obtained samples were transparent while others were opaque.

Table 1 Nominal composition (mol%) of the studied glasses

Glass No	SiO_2	PbO	Na_2O	Fe_2O_3
F0	50	25	25	–
F0.25	50	25	24.75	0.25
F0.5	50	25	24.50	0.5
F1	50	25	24	1
F3	50	25	22	3
F5	50	25	20	5
F7	50	25	18	7
F10	50	25	15	10
F15	50	25	10	15
F16	50	25	9	16
F20	50	25	5	20

Optical absorption measurements were carried out on the transparent polished rectangular samples of dimensions 3 × 10 × 30 mm using Jasco V-530 spectrophotometer in the range 190–1100 nm.

FTIR measurements were carried out on powdered samples after being mixed with KBr and pressed into discs. FTIR-6100 Jasco instrument was used for measuring the transmittance in the range 400–4000 wave number cm^{-1}.

X-ray powder diffraction (Bruker Axs, D8-Advance - X-ray Diffractometer, Germany) with Cu-target Cu Kα radiation with λ = 1.5405 Å, was used to identify the nature of the samples.

Archimedes method was used for density measurement using xylene of density (0.86 gcm^{-3}) as the immersing liquid. The density was calculated according using the equation: $D = (W_{air} / W_{air} - W_{xylene}) \times \rho_{xylene,}$ where W_{air} and W_{xylene} are the weight of the glass sample in air and in xylene, respectively, and ρ is the density of xylene.

The electrical measurements were performed on the prepared samples after painting their opposite sides with silver paste. Measurements were carried out using a programmable automatic LCR HiTester (HIOKI, 3532-50), Japan over a frequency range from 0.042 kHz to 1 MHz and temperature range from 25 to 300 °C. The temperature was determined using a copper/Constantan thermocouple in close proximity to the sample. The dielectric constant (ε′), the loss tangent (tan δ), and the ac conductivity (σ_{ac}) were determined based on the following expressions [29, 30]:

$\varepsilon' = C\ d\ /\ \varepsilon_o\ A,\ \varepsilon'' = \varepsilon'\ tan\ \delta,\ \sigma_{ac} = \omega\ \varepsilon_o\ \varepsilon''$, where C = measured capacitance of the sample (F), d = thickness of the sample (m), ε_o = permittivity of free space equals 8.85×10^{-12} F m $^{-1}$, A = Sample surface area (m^2), ω = the angular frequency, tan δ = the loss tangent which is obtained directly from the instrument.

3 Results and discussion

3.1 Optical studies

Figure 1 shows the absorption spectra of the transparent glass samples F0, F0.25, F0.5, F1 and F3. Samples with higher content than 3 mol% Fe_2O_3 were opaque (blackish-brown) that makes absorption measurement very difficult (samples thickness 3 mm). From Fig. 1 it can be noticed that the base glass F0 has UV-cut off at 339 nm, which is associated with *s2* lone pair electrons (s2 → s1p1) in Pb^{2+}, and no absorption bands in the visible region. Upon the addition of Fe_2O_3 and increasing its content at the expense of Na_2O the UV-cut off shifts to higher wavelengths. This shift can be ascribed to the $O^{2-}2p$–$Fe^{3+}3d$ charge transfer in octahedral coordinated Fe^{3+} ions [13], which increases as the Fe_2O_3 content replacing Na_2O increases. Charge transferring can also associate with adjacent redox species of iron (Fe^{2+}–O^{2-}–Fe^{3+}) where the relevant electronic orbital involves both the ferrous to ferric species. It is reported that, both ferrous and ferric ions absorb UV light below 350 nm due to the charge transfer process [31, 32].

The spectra of glasses F0.25 and F0.5 show bands at 379 nm (obscured in F0.5 due to the shift of its UV cut off), 402 and 445 nm, due to d-d transitions of Fe^{3+} ions in FeO_6 units [33]. These bands cannot be observed in the spectra of other glasses due to the red shift of their UV cut off. When the iron oxide content was increased to 1 mol% two bands could be observed in the visible region at 511, 662 nm and one near the infrared region at 949 (nm). Upon further increase of the iron oxide content to 3 mol % in glass F3, the band at 511 nm is obscured, while that at 949 nm becomes more developed. The band at 949 nm can be correlated with that due to Fe^{2+} ions appeared at 1050 nm in some sodium silicate glasses containing Fe_2O_3 [31, 34, 35]. The more development of the band at 949 nm in glass F3 indicates the increase of Fe^{2+} ions as the Fe_2O_3 content increases on the expense of Na_2O. The band at 511 nm can be correlated with that recorded around 530 nm due to Fe^{3+} in lead oxyfluoro silicate glasses [6]. Its development at shorter wavelength in the present glasses can be attributed to the replacement of fluoride by oxygens legends. The band at 662 nm in the spectra of glasses F1 and F3 was assigned to Fe^{3+} in octahedral coordination [24].

From the optical measurements of sample with up to 3% Fe_2O_3 it can be noticed that iron ions exist as Fe^{3+} and Fe^{2+} states and the latter state increases as the Fe_2O_3 content increases on the expense of Na_2O.

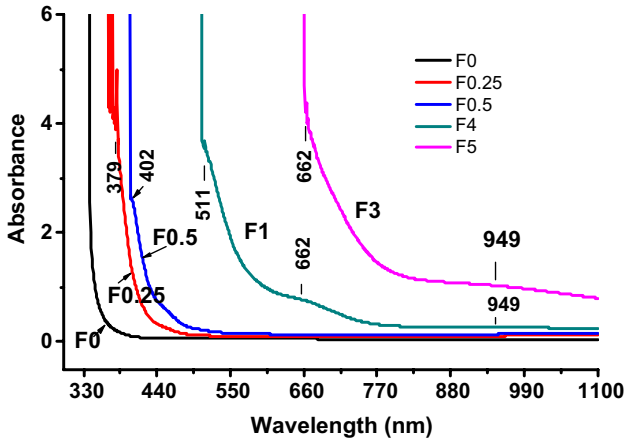

Fig. 1 The optical absorption of glasses F0, F0.25, F0.5, F1 and F3

3.2 Infrared spectra

The transmission infrared spectra of the studied samples in the range 400–4000 cm $^{-1}$ are illustrated in Fig. 2. The main structural vibrations are located in two regions: 400–600 and 600–1400 (cm $^{-1}$).

The first region (Fig. 2b) includes complex band with peaks at 486 and 426 cm^{-1}. The first band is due to bending Si–O–Si bonds in SiO_4 tetrahedra [36, 37], while the peak at 426 cm^{-1} is attributed Fe–O bonds in FeO_6 groups [38] overlapped with Pb–O vibrations in PbO_4 units [39, 40]. The area under this complex band decreases and its peaks decrease in intensity as the Fe_2O_3 content increases which may be due to decrease in the number of Si–O–Si bond vibrations in SiO_4 tetrahedra which may indicate a decrease in the SiO_4 units. It can also noticed that the peaks at 486 cm^{-1} shifts to lower wavenumber at 465 cm^{-1} in sample F20 which may reflect loosening in the glass structure. The band at 426 cm^{-1} shows a shift to higher wavelengths as the Fe_2O_3 content increases. It reaches 440 cm^{-1} in sample F20. This behavior can be attributed to the formation of FeO_4 at the expense of FeO_6 [38].

In the second region (600–1400 cm $^{-1}$) it can be noticed (Fig. 2b) that a symmetric stretching vibration of Si–O–Si bridging oxygen between tetrahedral SiO_4 is demonstrated by the band at 618–605 cm^{-1} [41] in glasses with greater than 15 mol% Fe_2O_3 (F15, F16, F20). This band cannot be noticed in other samples due to the high intensity of the neighboring band in the range 754–762 cm^{-1}. The band at 754 cm^{-1} (in glass F0) is assigned to Si–O–Si asymmetrical stretching vibration [42] overlapped with Si–O–Pb vibration [43]. The decrease of this band, particularly in samples F15, F16 and F20 enabled the appearance of the bands in the range 618−605 cm^{-1}. Asymmetric stretching vibration of Si-O-Si bonds in SiO_4 units are demonstrated by the bands at 971 cm^{-1} [44, 45] and the bands in the region 1121−1054 cm^{-1} [46]. The bands in the range 855–927 cm^{-1} are assigned to asymmetrical stretching vibrations of Si–O terminals [45] overlapped with Si–O–Pb bonds [47]. The shift of the band at 855 cm^{-1} in glass F0

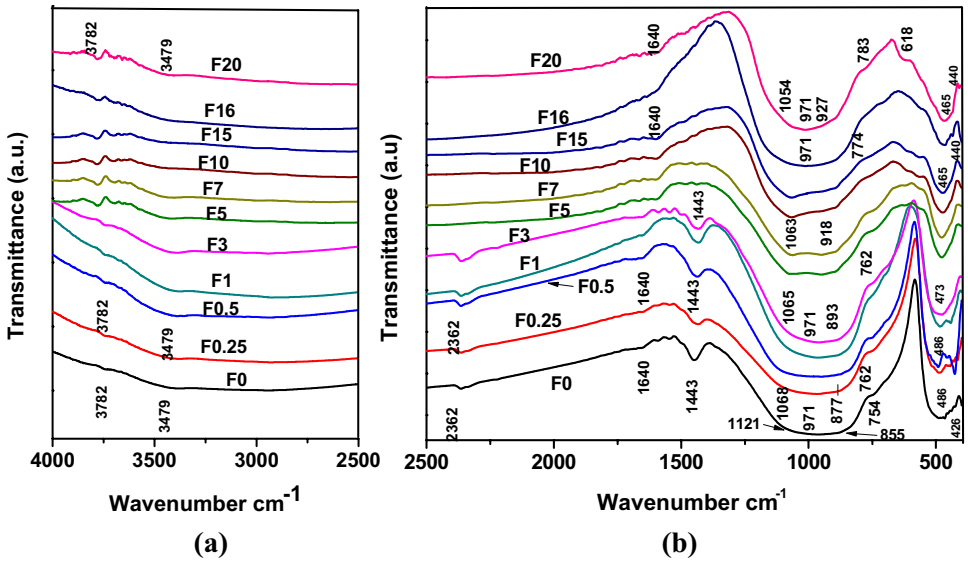

Fig. 2 Infrared transmittance spectra of the studied samples; (**a**) in the range 4000−2500 $cm^{-1}$and (**b**) in the range 2500−400 cm^{-1}

to higher frequency at 927 cm^{-1} in glass F20 can be attributed to the formation of non-bridging oxygens (NBO) with higher covalence.

From above discussion the SiO_4 units dominate in sample F0 as demonstrated by the broad band in the region 600–1400 cm^{-1} (Fig. 2b). The decrease in the width of this broad band confirms the decrease of the SiO_4 units upon substituting increasing amounts of Fe_2O_3 for Na_2O.

Some absorption bands due to unavoidable adsorbed water molecules on the grain surfaces of the samples during their preparation for FTIR measurements are noticed. The bands at 1443 cm^{-1} for samples F0–F3 (Fig. 2b) are ascribed to bending modes of O–H [48]. This band is not recorded for samples with Fe_2O_3 higher than 7 mol%, which indicates better weathering resistant as the amount of Fe_2O_3 replacing Na_2O increases. The 1640−1614 cm^{-1} (Fig. 2b) are attributed to bending modes of H–O–H [49] while those at 2362 cm^{-1} (Fig. 2a, b), 3462, 3479, and. 3782 cm^{-1} are attributed to stretching vibration bands of O–H in molecular H_2O [50].

3.3 Experimental and theoretical densities

Figure 3a shows the experimental densities of the studied glasses. It can be noticed that the experimental density progressively increased up to sample F15 after which the increment rate of the density was increased with increasing iron oxide content up to F20. The theoretical density calculated using Huggins and Sun factors [51] shows (Fig. 3b) a progressive increase in density up to glass F20. This behavior

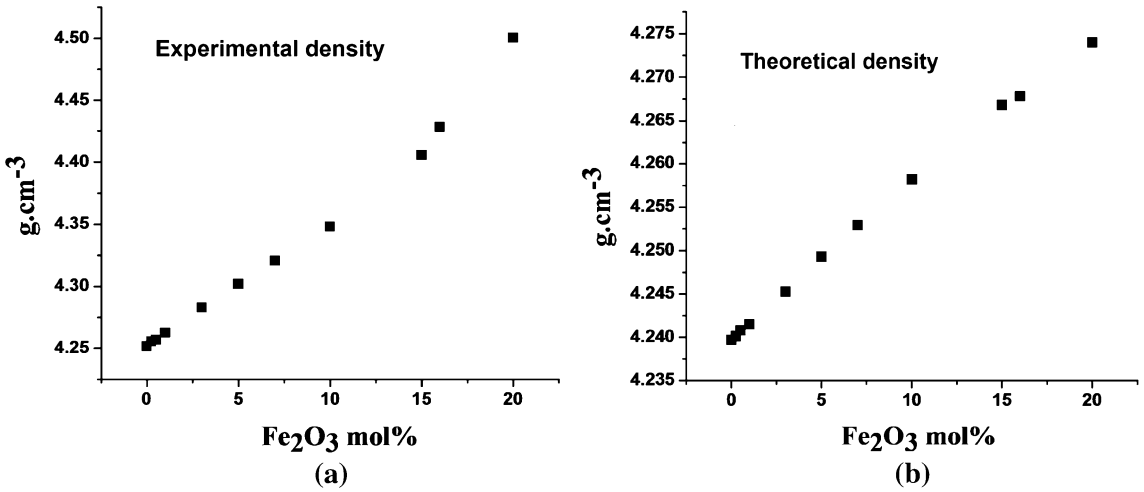

Fig. 3 Variation of (**a**) experimental density and (**b**) theoretical density with Fe_2O_3 content, replacing Na_2O for the glass samples studied

differs from that of the experimental density, which may relate to changes in glass structure, particularly above 15 mol% Fe_2O_3. The calculated density depends mostly on the coordination geometry of the metal cations [51]. The weight factor may play the main role which caused the density to increase with higher rate. The observed deviation above 15 mol% Fe_2O_3 in the relation of density versus Fe_2O_3 content is in accordance with the observed variation of the FTIR behavior above 15 mol% Fe_2O_3. Table 2 lists the measured and the calculated theoretical density of the glasses studied.

3.4 XRD

The XRD of glass samples F7, F10, F15, F16 and F20 are presented in (Fig. 4). The first sample is representative for samples from F0 to F5. The XRD patterns of these samples indicate that they are mostly amorphous, however XRD patterns of samples F16 and F20 consist of amorphous halo and a few reflexes characteristic of crystalline phases in these samples. Small reflexes which correspond to the XRD pattern of hematite can be detected. In sample F20 and F16 the presence of lines at 2θ = 22.61°, 33.00°, 39.1°, 41.22° (41.84° for sample F16), 49.44°, 54.52°, 56.67° (59.90° for sample F16) are in good agreement with those of hematite α-Fe_2O_3 (JCPDS, PDF Nos., 85–0599 and 24–0072). The present findings are consistent with those obtained by other authors [52, 53]. From the experimental density (Fig. 3a) the increase in the increment rate of the density of samples with 15% Fe_2O_3 or more may indicate that denser glass structures are formed. The crystalline phases revealed by XRD may explain such increase in the higher rates in density. Accordingly, the formation of FeO_4 units, as revealed by FTIR, and cross linking of the network of glass samples with more than 15 mol% Fe_2O_3 may enhance the formation of the hematite phase.

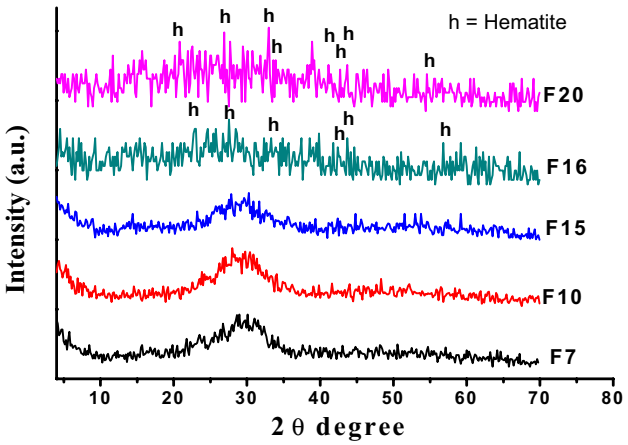

Fig. 4 XRD patterns of samples F7, F10, F15, F16 and F20

3.5 Electrical and dielectric properties

3.5.1 Dielectric behavior

Figure 5 shows the variation of dielectric constant with temperature as a function of Fe_2O_3 content, replacing Na_2O at two frequencies 100 kHz and 1 MHz. The values of ε' are almost constant for glass samples except for F16 and F20. The almost constant ε' for glass samples from F0 to F15 indicates that the short range displacement of ions may be involved. The temperature dependence of ε' for $Fe_2O_3 > 15$ mol% indicates that the movement of heavy dipoles was facilitated by weakening of bonds in the glass network with the increase of temperature [38]. The dielectric constant of samples F0, F0.25, F0.5, F1, F3, F5, F7, F10 and F15 shows weak variations. For example, they have average values of 12.16, 12.41, 12.75, 13.25, 14.09, 14.70, 14.78, 16.35, and 16.34, respectively at 1 MHz and temperature up to 300 °C, while for samples F16 and F20 the values of ε' increase from −115 to

Table 2 Experimental density, theoretical density calculated by Huggins and Sun factors [51], activation energy and dielectric constant (ε') of the studied glasses

Glass code	Density		Activation energy (eV)		ε' at 25 °C	
	Experimental	Theoretical	100 kHz	1 MHz	100 kHz	1 MHz
F0	4.2515	4.2397	2.37	1.74	13.90	9.99
F0.25	4.2553	4.2401	1.68	1.67	14.73	10.51
F0.5	4.2568	4.2408	1.51	1.50	15.75	11.18
F1	4.2625	4.2415	1.33	1.15	16.82	11.98
F3	4.2828	4.2453	0.96	0.58	17.96	13.08
F5	4.3019	4.2493	0.69	0.51	18.89	13.50
F7	4.3205	4.2529	0.49	0.43	19.43	13.90
F10	4.3481	4.2582	0.47	0.58	21.03	14.90
F15	4.4057	4.2668	0.45	0.40	22.00	15.14
F16	4.4284	4.2678	0.36	0.16	132.60	115.07
F20	4.5002	4.2740	1.91	1.56	43.87	33.84

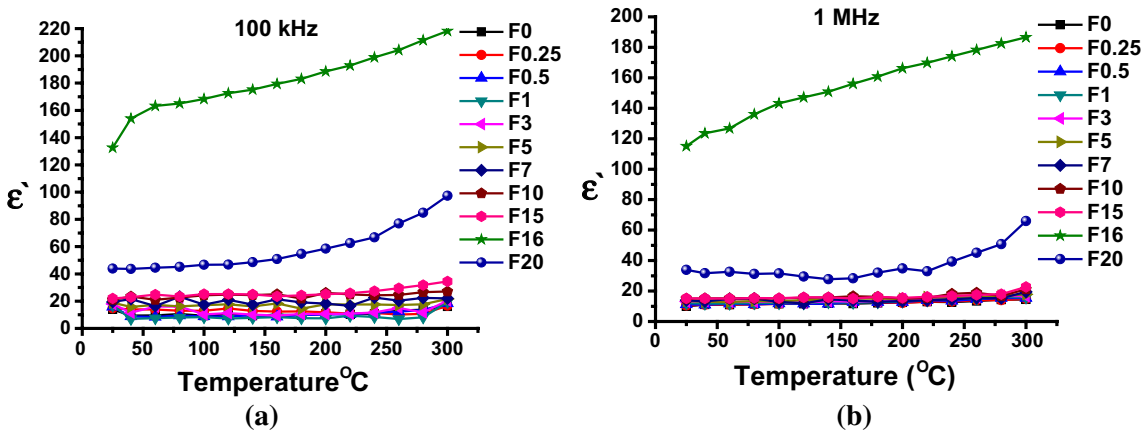

Fig. 5 Variation of dielectric constant with temperature at (**a**) 100 kHz and (**b**) 1 MHz for the glass samples studied

186 and from −34 to 66, respectively, at 1 MHz and temperature up to 300 °C.

Figure 6 shows the variation of dielectric constant with Fe_2O_3 content, replacing Na_2O at the frequencies 50 Hz, 100 Hz, 500 Hz, 1 kHz, 10 kHz, 50 kHz, 100 kHz, 500 kHz, 800 kHz and 1 MHz, at two temperatures (25 and 300 °C). It can be noticed that the dielectric constant increases to a maximum with the increasing of the iron oxide content. For example, for sample F0 the ε' increases from 13.90 to reach a maximum value of 132.60 for sample F16 then it decreases to 43.87 at 100 kHz and 25 °C. This decrease in the dielectric constant after reaching maximum values with increasing $Fe_2O_3 > 15$ mol% can be attributed to the decrease of Fe^{3+} ions contributing in the conduction mechanism as a result of increasing the proportion of Fe^{3+} states in network forming positions [54]. The present attribution is consistent with the above obtained IR results where more Fe^{3+} ions are likely to be introduced as NWF in glasses with 20 mol% Fe_2O_3.

From Fig. 6 it can be noticed that the values of ε' at 100 kHz or lower frequencies are generally higher than those at higher frequencies up to 1 MHz (Fig. 6) particularly for glasses F16 and F20. It is worth noticing that the dielectric constant decreases as the measurement is carried out at higher frequencies, which can be attributed to the slow response of the heavy dipoles behind the external field [38, 55, 56].

3.5.2 *Electrical conductivity*

The introduction of transition metal ions (TMI) with more than one valence state in glass exhibited semiconducting properties [57–59], where conduction can occur by electron transfer from ions in the lower valence state to those in a higher valence state [58, 60]. Figure 7 shows the variation

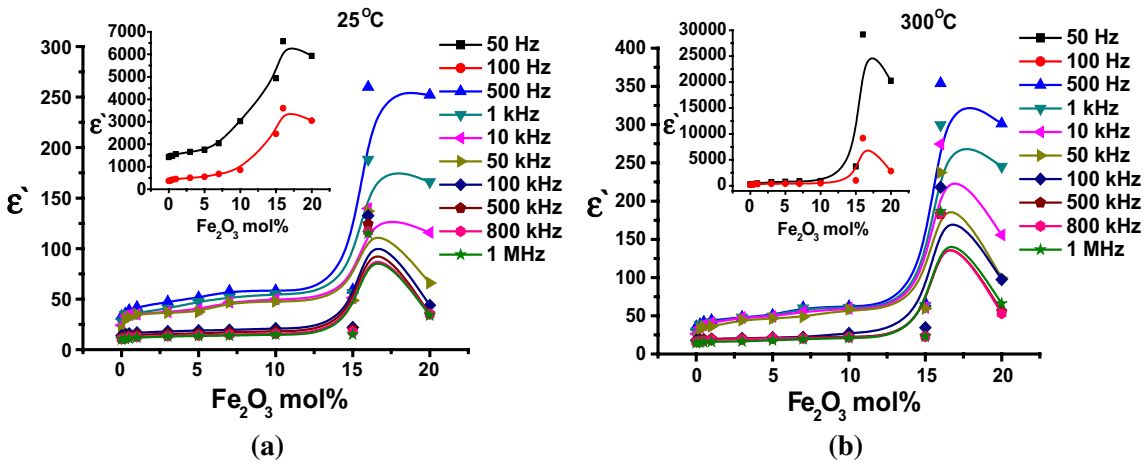

Fig. 6 Variation of the dielectric constant with Fe_2O_3 content, replacing Na_2O for different frequencies at (**a**) 25 °C and (**b**) 300 °C

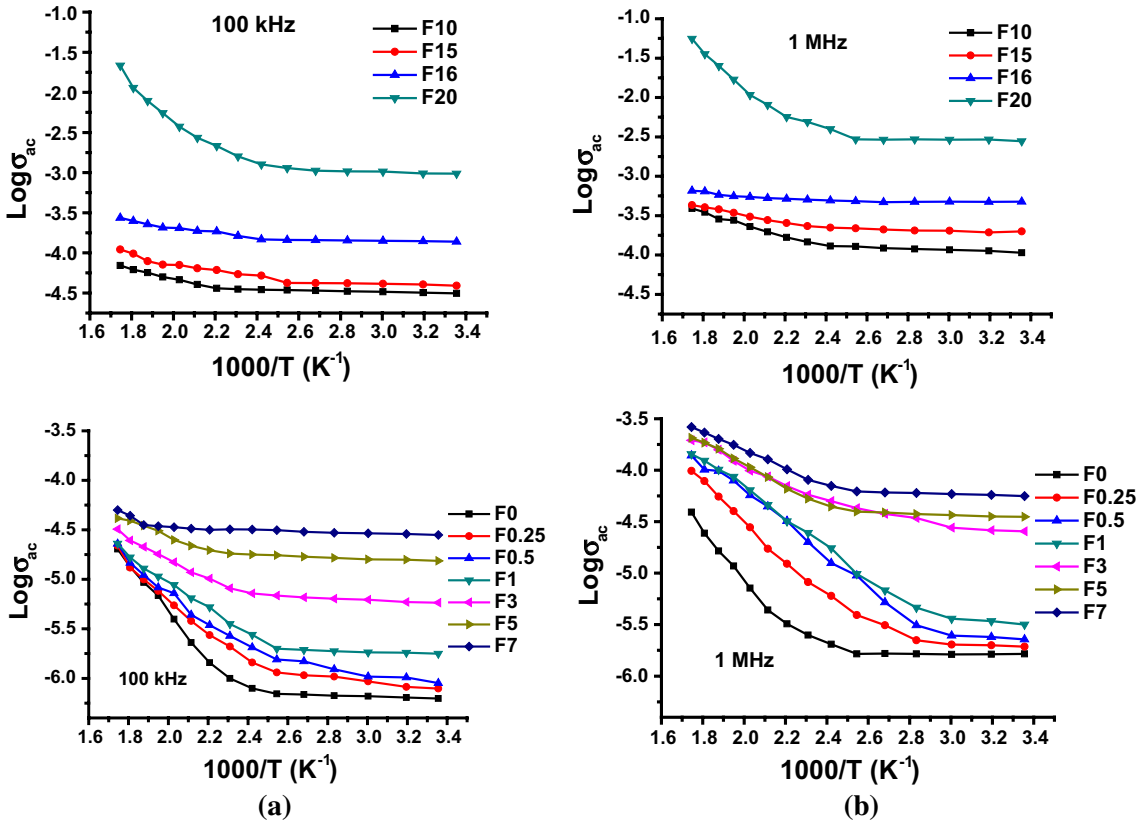

Fig. 7 Variation of log σ_{ac} of the glasses studied as a function of inverse temperature (T) at (**a**) 100 kHz and (**b**) 1 MHz The results of samples with Fe_2O_3 content higher than 7 mol% are drawn separately for clarity

of the logarithm of ac conductivity of the glasses studied as a function of inverse temperature (T) at 100 kHz and 1 MHz. It can be seen that the conductivity increases by raising the temperature. The plots of logσ_{ac} versus inverse temperature show two parts at low and high temperature regions. The values of the activation energy of those in the high temperature region have been determined from their slopes and listed Table 2. From this table it can be seen that the activation energy is significantly reduced from the range 2.37–1.74 eV to the range 0.36–0.16 eV for samples F0 and F16, respectively, then it is increases to the range 1.91–1.56 eV for sample F20. The values of activation energies for glasses F0, F0.25, F0.5, F1 and F3 reveal that their conduction is mainly ionic in nature, while glasses F5, F7, F10, F15 and F16 have lower values indicating the dominant of electronic conduction. The lowest activation energy of glass F16 which reached 0.36 eV (at 100 kHz) or 0.16 eV (at 1 MHz), can be attributed to the dominant and the increase of the electron charge carriers. For glass F0 the high activation energy (2.37 or 1.74 eV at 100 kHz and 1 MHz, respectively), can be explained on the bases of the above obtained FTIR results. The dominate of the SiO_4 units with bridging oxygens and the absence of iron ions in the composition of this glass (F0) results in the higher energy needed for migration of the charge carriers. The conduction seems to proceed via electronic at the low temperature regions and via ionic conduction in the high temperature region. These results are consistent with published data [61]. The increase of the electronic conduction upon increasing the iron oxide content above 1 mol% seems to be related to the more increase of Fe^{2+} ions. When glass containing Fe_2O_3 is melted at high temperature, part of ferric ions (Fe^{3+}) are converted into the divalent state (Fe^{2+}): $Fe^{3+} \rightarrow Fe^{2+} + e$. Usually, iron occurs in silicate glasses in equilibrium between Fe^{3+} and Fe^{2+} ions, where their ratio Fe^{2+}/Fe^{3+} is a function of glass composition, pressure, temperature and oxygen fugacity [62]. When melting of such glasses is carried out in the presence of a reducing material such as Pb [5], the prepared glasses are expected to contain relatively high Fe^{2+} content, consequently the electron hopping between Fe^{2+} and Fe^{3+} Increases. The increased activation energy in the high temperature region for glass F20 (Table 2) to values of 1.91 or 1.56 eV can be attributed to the re-participation of the ionic conduction which needs relatively high activation energy.

Figure 8 shows that the conductivity of the glass samples increases with increasing of Fe_2O_3 content at 25 and 300 °C. The increase in ac conductivity with increasing

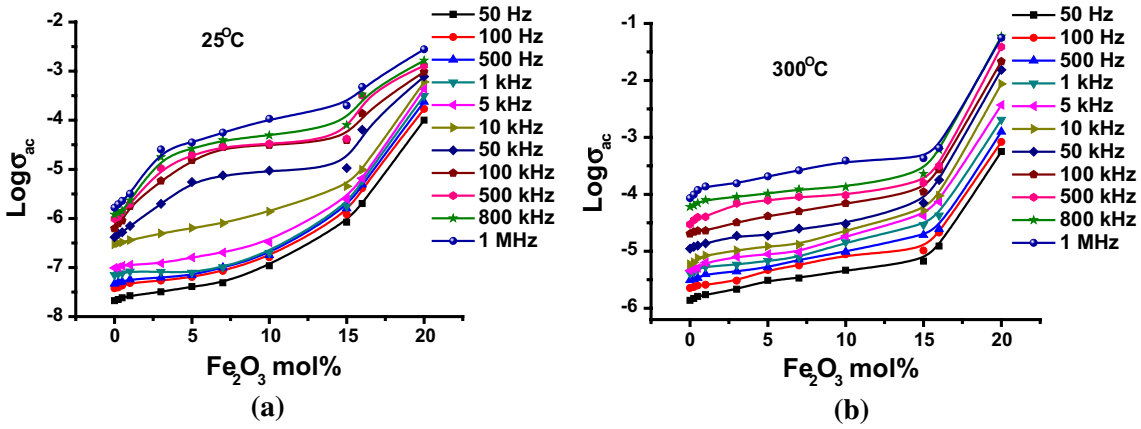

Fig. 8 Variation of log σ_{ac} with iron oxide content at different frequencies at (**a**) 25 °C and (**b**) 300 ºC

Fe_2O_3 content that replacing Na_2O can be attributed to the increase of charge carriers. It can be noticed that the increase in conductivity is accompanied by a decrease in activation energy (Table 2) with increasing Fe_2O_3 content. This behavior is consistent with several published data for glasses containing transition metal oxide [63–65]. At 100 kHz and at 25 °C, the conductivity is increased from 6.24×10^{-7} to 9.69×10^{-4} S/cm for samples F0 and F20, respectively, while at 300 °C it increased from 2.02×10^{-5} to 2.15×10^{-2} S/cm for samples F0 and F20, respectively. The conduction in the present glasses—containing Fe_2O_{3-} seems to be a combination of ionic and electronic controlled by electron hopping between Fe^{2+} and Fe^{3+} sites. It can also be noticed (Fig. 8a, b) that the conductivity increases with increasing the frequency. The increase of conductivity with increasing frequency confirms the semiconducting nature of the studied glasses.

4 Conclusions

Glass of the composition (mol%) (25–x) Na_2O–xFe_2O_3–25PbO–50SiO_2, where x = 0, 0.25, 0.5, 1, 3, 5, 7, 10, 15, 16 and 20 (mol%) were prepared by the melt quenching method.

Replacing Fe_2O_3 for Na_2O affect the optical properties as a result of the contribution of Pb^{2+}, Fe^{2+} and Fe^{3+} ions. Absorption bands due Fe^{3+} and Fe^{2+} oxidation states are recorded in the visible and near IR regions. The optical measurements revealed that iron ions exist as Fe^{2+} state increases, as the Fe_2O_3 content increases at the expense of Na_2O.

The FTIR indicates that replacement of Na_2O by ≥15 mol% Fe_2O_3 produces structural changes, where the SiO_4 units decrease and FeO_4 units increase. It also indicates that samples with better weathering resistant are obtained as the amount of Fe_2O_3 replacing Na_2O increases.

XRD indicated change in the amorphous state after replacement Na_2O by ≥15 mol% Fe_2O_3, where the sample with Fe_2O_3 content of 20 mole% exhibits crystals of hematite phase to be formed in a glassy matrix.

The electrical conductivity vs. reciprocal temperature revealed two parts at low and high temperature region. So, electrical conduction in the studied glasses seems to proceed by ionic and electronic controlled by electron hopping between Fe^{2+} and Fe^{3+} sites. The activation energy of electrical conduction at the high temperature region decreased from 1.74 eV for glass sample of un-replaced Na_2O to 0.16 eV (at 1 MHz) as the amount Fe_2O_3 replacing Na_2O was increased to 16 mol% Fe_2O_3. The electrical conduction is mainly electronic in nature as the Na_2O replaced by Fe_2O_3 increases to 16 mol% and above this concentration both mechanisms the ionic and electronic proceed.

The dielectric constants of samples with replaced $Na_2O < 16$ mol% Fe_2O_3 show weak variation which reveal high thermal stability in the studied range of temperature. They have average values in the range of 12–16 measured at 1 MHz and temperature up to 300 °C. Samples with 16 and 20 mol% Fe_2O_3 show high ε' values of 115 to 186 and from 34 to 66, respectively, at 1 MHz and temperature up to 300 °C. These results represent promising candidates for the studied glasses to be used as energy storage materials in electronic devices.

Acknowledgements The authors acknowledge the financial support of this work from the National Research Centre, 33 E l Bohoth St. (former El Tahrir St.), Dokki, Giza P.O. 12622, Egypt, under Contract No. P 100910/ 2015–2016.

References

1. G.P. Kothiyal. S.V. Phadnis, V.K. Shrikhande, T. Mirza, M.K. Totlani, V.C. Sahni, Anti-Corros Methods Mater. **47**, 280 (2000).
2. S.P. Singh, R.P.S. Chakradhar, J.L. Rao, B. Karmakar, J. Alloys Compd. **493**, 256 (2010)
3. T. Komatsu, Mohiri H., Phys. Chem. Glasses **40**, 257 (1999).
4. A. M. Zahra, Zahra C.Y., Piriou B., J. Non-cryst. Solids **155**, 45 (1993).
5. N.K. Sanjay, A. Agarwal, Ind. J. Pure Appl. Phys **48**, 205 (2010)
6. T.G.V.M. Rao, A. R. Kumar, B. H. Rao, N. Veeraiah, M. R. Reddy, J. Molec. Struct. **1021**, 7 (2012).
7. P.W. Wang, L. Zhang, J. Non-Cryst. Solids **194**, 129 (1996)
8. J. Rybicki, A. Rybicka, A. Witkowska, G. Bergmanski, A. Di Cicco, M. Minicucci, G. Mancini, J. Phys. **13**, 9781 (2001)
9. P.R. Rao, L. Pavić, A. Moguš-Milanković, V. Ravi Kumar, I.V. Kityk, N. Veeraiah, J. Non-Cryst. Solids **358**, 3255 (2012)
10. N.C.R. Babu, M.A. Valente, N.N. Rao, M.P.F. Graça, G.N. Raju, M. Piasecki, N. I.V. Kityk, Veeraiah. J. Non-Cryst. Solids **358**, 3175 (2012)
11. B. Mehdikhani, G. H. Borhani, Process. Appl. Ceram. **7**, 117 (2013).
12. B.O. Mysen, D. Virgo, E.R. Neumann, F.A. Seifert, Am. Mineral **70**, 317 (1985)
13. T. Uchino, K. Nakaguchi, Y. Nagashima, T. Kondo, J. Non-Cryst. Solids **261**, 72 (2000)
14. B.O. Mysen J. Non-Cryst. Solids **95–96**, 247 (1987)
15. B. Hannoyer, M. Lenglet, D. Durr, R. Cortes, J. Non-Cryst. Solids **151**, 209 (1992)
16. C. Weigel, L. Cormier, G. Calas, D.T. L.e Galoisy, Bowron. J. Non-Cryst. Solids **354**, 5378 (2008)
17. G. Ottonello, R. Moretti, L. Marini, M.V. Zuccolin, Chem. Geol. **174**, 157 (2001)
18. J.A. Tangeman, R. Lange, L. Forman, Geochim. Cosmochim. Acta **65**, 1809 (2001)
19. R. Klement, J. Kraxner, M. Liška, Ceramics–Silikáty **53**, 180 (2009).
20. F. Abdel-Wahab, A.G. Mostafa, A.E. Belal, E.M. El-Agwany, Mater. Chem. Phys. **93**, 243 (2005)
21. D.P. Singh, G.P. Singh, J. Alloys Compd. **546**, 224 (2013)
22. J. Coelho, C. Freire, S. N. Hussain. Spectrochimica Acta Part A **86**, 392 (2012)
23. R.P.S. Chakradhar, G. Sivaramaiah, J.L. Rao, N.O. Gopal. Spectrochimica Acta Part A **62**, 51 (2005)
24. M. Ookawa, T. Sakurai, S Mogi, T. Yokokawa, Mater Trans, JIM, **38**, 220 (1997).
25. R.J. Barczyński, N.A. Szreder, J. Karczewski, M. Gazda, Solid State Ionics **262**, 801 (2014)
26. F. Pinakidou, M. Katsikini, P. Kavouras, F. Komninou, Th. Karakostas, E. C. Paloura, J. Non- Cryst. Solids, **354**, 105 (2008).
27. H. Hagiwara, R. Oyamada, Yogyo-Kyokai-Shi **84**, 264 (1976).
28. S. Ibrahim, Morsi M. Morsi, Mater. Chem. Phys. **138**, 628 (2013)
29. T. Sankarappa, M. Prashant Kumar, G.B. Devidas, N. Nagaraja, R.R. Reddy, J. Mol. Struct. **889**, 308 (2008)
30. B. Kumar, T. Vijaya, M. Sankarappa, S. Kumar, P.J.P. Kumar, R. Sadashivaiah, R. Reddy, Phys. B **404**, 3487 (2006).
31. C.R. Banford, Glass Science and Technology, Colour Generation and Control in Glass. (Elsevier, Amsterdam, 1977)
32. W.A. Weyl, Society of Glass Technology, Coloured Glasses London, (1951)
33. B. Mirhadi, J. B. Mehdikhani, Korean Ceram. Soc. **48**, 117 (2011)
34. S.B. Donald, A.M. Swink, H.D. Schreiber, J. Non-Cryst. Solids, **352**, 539 (2006).
35. K.R. Kukadapu G.L Li H. Smith, J. Non-Cryst.. Solids **317**, 301(2003).
36. S.A. MacDonald, C.R. Schardt, D.J. Masiello, J.H. Simmons, J. Non-Cryst. Solids **275**, 72 (2000)
37. A.M.B. Silva, C.M. Queiroz, S. Agathopoulos, R.N. Correia, M.H.V. Fernandes, J.M. Oliveira, J. Mol. Struct. **986**, 16 (2011)
38. R. Hisam, A.K. Yahya, H. M. Kamari, Z. A. Talib. R. H. Y. Subban Mater. Express, **6**, 149 (2016).
39. M. Bosca, L. Pop, B. Ghe, P. Pascuta, E. Culea, J. Alloys Compd. **479**, 579 (2009)
40. O.C. Mocioiu, M. Popa, E.I. Neacsu, M. Zaharescu, J Non-Cryst. Solids. **361**, 130 (2013).
41. G. Kaur, M. Kumar, A. Arora, O.P. Pandey, K. Sinh, J. Non-Cryst. Solids **357**, 858 (2011)
42. R. D. Husung Robert H. Doremus, J. Mater. Res. 5, 2209 (1990).
43. B. Karmakar, R.N. Dwivedi, J. Non-Cryst. Solids **342**, 132 (2004)
44. M.T. Wang, J.S. Cheng, M. Li, F. He, Physica B **406**, 187 (2011)
45. L. Stoch, M. S´roda, J. Molec. Struct. **511–512**511–512, 77 (1999).
46. E.C. Ziemath, M.A. Aegerter, J. Mater. Res. **9**, 216 (1994)
47. T. A. Sidorov, Zhurnal Prikladnoi Spektroskop ii **6**, 98(1967).
48. H. Moor, P.W. McMillan, J. Soc. Glass Technol. **40**, 97 (1956).
49. C.I. Merzbacher, W.B. White, J. Non-Cryst. Solids **130**, 18–34 (1991)
50. G. Navara, J. Non Cryst Solids **353**, 555 (2007)
51. M.L. Huggins, K. H. Sun, J. Am.Ceram.Soc.26,4(1943), in Handbook of Glass Manufacture (Compiled and Edited by F.V. Tooley, Ogdin Pub. Co. ,N.Y.(1953) P.25
52. M. S. Islam, J. Kurawakia, Y. Kusumoto, M. A. Al-Mamun, M. Z. Bin Mukhlish, J. Sci. Res. **4**, 99(2012).
53. S.K. Sahoo, K. Agarwal, A.K. Singh, B.G. Polke, K.C. Raha, Int. J. Eng. Sci. Technol. **2**, 118 (2010)
54. S. Yusub, G.S. Baskaran, S.B.M. Krishna, C.H. Rajyasree, A.R. Babu, D.K. Rao, Ind. J. Pure Appl. Phys. **49**, 315 (2011)
55. N.D. Sankyr, E. Aydyn, M. Sankyr, Int. J. Electrochem. Sci. **9**, 3864 (2014)
56. R.M.M. Morsi, A.M. Abdelghany, M.M. Morsi, J Mater Sci. **26**, 5120 (2015)
57. M.A. Sidkey, A.A. El-Moneim, L.A. El-Latif, Mater. Chem. Phys. **61**, 103 (1999)
58. M.M. El-Desoky, J. Non-Cryst. Solids **351**, 3139 (2005)
59. V. Rajendran, N. Palanivelu, B.K. Chaudhuri, K. Goswami, J. Non-Cryst. Solids **320**, 195 (2003)
60. S. Annamalai, R.P. Bhatta, I.L. Pegg, B. Dutta, J. Non- Cryst. Solids **358**, 1380 (2012)
61. A.G. Mostafaa, A.H. El-Dosokey, K.H. Idress, H.M. Goumaa, Int. J. Res Eng. Sci. (IJRES) **2**, 58 (2014)
62. E.S. Dunaeva, I.A. Uspenskaya, K.V. Pokholok, V.V. Minin, N.N. Efimov, E..A. Ugolkova, E. Brunet, J. Non-Cryst.Solids **358**, 3089 (2012).
63. A. Al- Hajry, A.A. Soliman, M.M. El- Desoky, Thermochim Acta **427**, 181 (2005)
64. M.M. El-Desoky, J. Mater. Sci. **14**, 215 (2003)
65. M.M. El-Desoky, I. Kashif, Phys. Stat. Sol. (a) **194**, 89 (2002)